Reflective-Mode Phase-Variation Permittivity Sensor Based on a Step-Impedance Microstrip Line Terminated With a Slot Resonator for Solid and Liquid Characterization

Jonathan Muñoz-Enano, *Member, IEEE*, Paris Vélez, *Senior Member, IEEE*, Pau Casacuberta, *Graduate Student Member, IEEE*, Lijuan Su, *Member, IEEE*, and Ferran Martín, *Fellow, IEEE*

***Abstract*—This paper proposes a highly sensitive single-frequency microwave sensor for dielectric characterization of solids and liquids. The sensor is a reflective-mode one-port device consisting of a step-impedance microstrip line terminated with a slot resonator (the sensing element) transversely etched on the ground plane. The working principle of the sensor is the variation experienced by the phase of the reflection coefficient at the operating frequency as consequence of changes in the dielectric properties (dielectric constant) of the material under test (MUT), either a solid or a liquid, which should be in contact with the slot resonator. A relevant advantage of the reported sensor is the fact that the MUT is located in the back substrate side of the microstrip structure. Therefore, any potential interaction between the MUT, including the mechanic holder used for liquid sensing, and the microstrip line, is prevented. A detailed sensitivity analysis that takes into account the effects of losses is carried out. It is concluded that, depending on the losses of the MUT, there are two different sensor operation regimes (the low-loss and the high-loss regimes), with unequal behavior, but both useful to sensitively detect changes in the dielectric properties of the MUT. The maximum sensitivity in the prototype device devoted to the measurement of the dielectric constant in low-loss solid samples is 255.5º. In the liquid sensor, equipped with a 3D-printed holder, and focused in this paper on the detection of small volume fractions of isopropanol in DI water, the maximum sensitivity is 64.96º/%.**

***Index Terms*— Liquid sensor, microstrip, microwave sensor, phase-variation sensor, slot resonator, step-impedance transmission line.**

I. INTRODUCTION

SIGNIFICANT efforts have been recently dedicated to performance optimization in planar microwave sensors (see [1], [2], and references therein). In particular, sensor sensitivity is a fundamental parameter that determines the capability of the sensor to detect small changes in the input variable (designated as measurand). Among the different principles/strategies devoted to the implementation of planar microwave sensors, phase variation has been demonstrated to be a useful approach to achieve unprecedentedly high sensitivities [3]. There are many types of phase-variation sensors, including transmission-mode [4]-[12] and reflective-mode [3], [13]-[20] devices. In such sensors, the output variable is the phase of either the transmission or the reflection coefficient measured at a certain (operational) frequency. Thus, phase-variation sensors are single-frequency devices, an advantageous aspect as compared to frequency-variation sensors [21]-[31], or frequency-splitting sensors [32]-[36], which need frequency sweeping signals for sensing. Such signals are generated by means of voltage-controlled oscillators (VCO) in operational environment, and the requirements of such VCOs might be severe in terms of bandwidth, depending on the output dynamic range of the sensors.

Both phase-variation and frequency-variation (or frequency-splitting) sensors are robust against electromagnetic interference (EMI) and noise, as corresponds to the fact that phase and frequency are tolerant to their effects. By contrast, in the so-called coupling-modulation sensors [37]-[48], the typical output variable is a magnitude (of either a voltage or a transmission/reflection coefficient) measured at a certain operating frequency, less tolerant to EMI and noise. Thus, phase-variation sensors combine the advantages of frequency-variation and coupling-modulation sensor, i.e., robustness against EMI and noise, and operation at a single frequency. These two aspects, and the potentially achievable high sensitivity, make phase-variation sensors firm candidates for a

This work was supported by MCIN/AEI 10.13039/501100011033, Spain, through projects PID2019-103904RB-I00, PID2022-139181OB-I00 (ERDF European Union), and PDC2021-121085-I00 (European Union Next Generation EU/PRTR), by the AGAUR Research Agency, Catalonia Government, through the project 2021-SGR00192, and by Institució Catalana de Recerca i Estudis Avançats (ICREA). P. Casacuberta acknowledges the Ministerio de Universidades, Spain, for the FPU grant (Ayudas para la formación de profesorado universitario), ref. FPU20/05700. L. Su acknowledges the Juan de la Cierva Program for the support through the project IJC2019-040786-I. *(Corresponding author: J. Muñoz-Enano; e-mail: Jonatan.Munoz@uab.cat).*

The authors are with CIMITEC, Departament d'Enginyeria Electrònica, Universitat Autònoma de Barcelona, 08193 Bellaterra, Spain.

Color versions of one or more of the figures in this article are available online at http://ieeexplore.ieee.org.

diversity of applications.

Phase-variation sensors have been implemented by considering various approaches, including meander lines (to reduce the shape factor) [6], [8], artificial transmission lines [4], [7], [9], [10] (taking benefit of the high dispersion in such lines), step-impedance transmission line configurations (either in transmission [11], or in reflection [3], [13]-[16]), and coupled structures [19], [20] (it should be mentioned that many other sensors based on coupled structures, exploiting different principles, have been reported [49]-[57]). Among such different approaches, it has been shown that reflective-mode sensors based on a cascade of high/low-impedance inverters terminated with a planar resonator, either semi-lumped [15], [16] or distributed [3], [13], [14], can provide very high sensitivities. The impedance contrast of the inverters, implemented in practice with quarter-wavelength transmission line sections, is the reason for such sensitivity enhancement. However, up to date, all the considered implementations of these reflective-mode phase-variation sensors based on a step impedance configuration (high and low impedance inverters alternating) are terminated with a metallic resonator [3], [13]-[16].

In the present paper, a reflective-mode phase-variation sensor implemented by means of a cascade of high/low impedance inverters terminated with a slot resonator is proposed (this sensing resonant element has been chosen because the achievable sensitivity is superior to that achievable with other defect ground structure resonators, such as the complementary split ring resonator, CSRR, as discussed in [31] in reference to frequency-variation sensors). The paper is indeed an extension of the work [58], where a similar sensor devoted to the characterization of edible oils by usage was reported. Nevertheless, in this paper an accurate sensitivity analysis, taking into account the effects of MUT losses, is carried out. It is shown that, depending on the level of losses of the MUT, two different operation regimes can be distinguished, i.e., the low-loss regime, where the phase of the reflection coefficient, ϕ_ρ, decreases with the dielectric constant of the MUT, ε_{MUT}, and the high-loss regime, where ϕ_ρ increases when ε_{MUT} increases. Nevertheless, a high sensitivity can be achieved under operation in both regimes, as it will be shown. The main advantageous aspect of this sensor is the fact that the material under test (MUT) and associated mechanical accessories (e.g., the 3D-printed holder for the liquid sensor) are placed in the back substrate side, thereby avoiding any potential interaction with the microwave circuitry (step impedance configuration).

The work is organized as follows. Section II presents the proposed sensor, including the topology and the circuit model, which is validated by comparing electromagnetic simulations and circuit simulations with extracted parameters. Section III is focused on the analysis of the sensitivity. For that purpose, the circuit model, including losses, is considered. Such losses mainly account for the presence of potentially lossy samples, e.g., liquids, namely, it is assumed that the sensor structure is lossless, a reasonable approximation provided the sensor is implemented in low-loss microwave substrates. Nevertheless, if substrate losses are comparable to MUT losses, or even if radiation losses exist, all these losses can be accounted for by the same element in the model (a conductance). From that analysis, it will be concluded that the sensor can operate under two different operation regimes, depending on the level of losses, i.e., the low-loss and the high-loss regime. Moreover, it will be shown that the sensitivity can be enhanced through an adequate design, regardless of the specific mode of operation. Two prototype devices are presented and experimentally validated in Section IV. One of such sensors is devoted to the dielectric characterization of low-loss solid samples; the other one, operating under the high-loss regime, is focused on liquids. Section V compares the proposed sensors with other similar sensors reported in the literature. Finally, Section VI concludes the work.

II. Sensor Topology, Circuit Model, and Working Principle

Figure 1 depicts a typical topology and the equivalent circuit model of the sensor presented in this work. The sensing element is a slot resonator, etched in the ground plane, and modelled by the parallel resonant tank, with inductance, capacitance and conductance L, C and G, respectively. Such resonator is the termination of a high impedance quarter-wavelength transmission line (acting as impedance inverter), with impedance Z_1, used to boost up the sensitivity [3],[15]. Introducing a via in the transversal plane to the right of the slot resonator's position has the effect of grounding the resonator. Therefore, the equivalent circuit model is the one depicted in Fig. 1(b), where losses in the resonant tank have been included (by means of G), in order to take into account the presence of a potentially lossy sample in contact with the slot resonator (and eventually substrate losses, and even radiation losses).

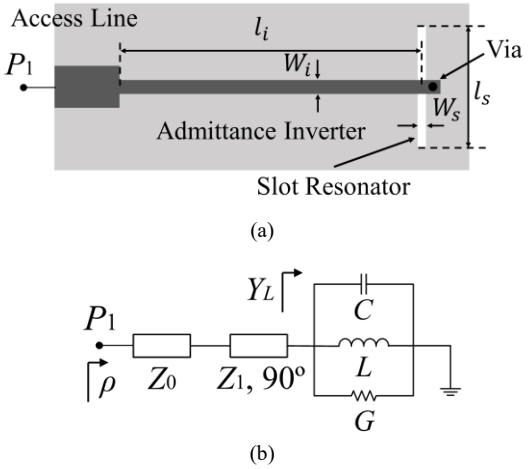

Fig. 1. Typical topology (a) and equivalent circuit model (b) of the proposed sensor. The admittance inverter is implemented by means of a quarter-wavelength (or 90º) line section. The effects of potential parasitic capacitances in the impedance discontinuities can be compensated with the length of the line sections and have been ignored to avoid an excessive complex circuit model. The good prediction of the sensitivity in the limit of small perturbations, as given by the sensitivity analysis to be discussed in Section III, verifies that such parasitic capacitances can be ignored. Note that the via connects the termination of the line to ground, just to the right of the transverse plane where the slot is placed.

The working principle of the sensor is the variation of the phase of the reflection coefficient at a fixed (operational) frequency caused by changes in the dielectric properties of the MUT, specifically the dielectric constant. The operational frequency, f_0, must be set to the resonance frequency of the slot resonator when it is loaded with the so-called reference (REF) sample. The reason is that, at this frequency, the phase slope roughly exhibits its maximum value, and this maximizes the sensitivity (or derivative of the phase of the reflection coefficient with the dielectric constant of the MUT) in the vicinity of the dielectric constant of the REF sample [3],[15]. The length of the high impedance line (inverter) must be set to the necessary value to exhibit an electrical length of 90º (a quarter-wavelength) at that frequency. Moreover, since the sensor operates at a single frequency, the via can be replaced with an open-ended quarter-wavelength transmission line, as it will be shown in Section IV, where specific prototypes are presented. This extends the overall dimension of the sensor, but does not represent an increase in the size of the sensing region, dictated by the slot resonator, and avoids the presence of a grounding via. Let us also mention that, in the topology of Fig. 1, a single impedance inverter has been considered. Nevertheless, it is possible to further boost up the sensitivity by cascading additional inverters with alternating low/high impedance [3],[15].

For circuit model validation, let us consider the topology of Fig. 1(a), including the via and excluding the access line, with dimensions W_i = 0.24 mm, l_i = 14.4 mm, W_s = 0.2 mm and l_s = 36 mm, and the characteristics of the *Rogers 4003C* substrate with dielectric constant ε_r = 3.55, thickness h = 1.524 mm, and loss factor tanδ = 0.0022. The dependence of the magnitude and phase of the reflection coefficient with frequency is depicted in Fig. 2 (for the purpose of circuit validation, it is assumed that the sensing resonator is surrounded by air). Parameter extraction has been carried out by identifying the resonance (angular) frequency of the bare resonator

$$\omega_0 = \frac{1}{\sqrt{LC}}. \tag{1}$$

At such frequency, the impedance seen from the input port is purely real and it is roughly a short circuit (due to the effects of the impedance inverter), and therefore the phase of the reflection coefficient is ϕ_ρ = ±180º. Thus, the resonance frequency can be identified by the phase jump in the phase response. Expression (1) is one condition that must satisfy the reactive parameters, L and C, of the model. Nevertheless, we need two additional conditions to univocally determining the three lumped-element parameters of the model. The phase slope at resonance provides the second condition. However, the analytical calculation of such phase slope, by considering that the inverter is implemented by means of a quarter-wavelength transmission line, is not straightforward. The calculation notably simplifies by situating the input port at the resonator's plane, i.e., by neglecting the presence of the quarter-wavelength (non-ideal) impedance inverter. Under these conditions, expression (1) is also valid, since the resonance frequency of the slot resonator does not depend on the presence of additional elements in the structure (nevertheless, at such frequency the phase of the reflection coefficient nulls, as corresponds to roughly an open termination). For the calculation of the phase slope (by excluding the high impedance and the access line sections), let us first obtain the reflection coefficient, given by

$$\rho = \frac{Y_0 - Y_L}{Y_0 + Y_L} \tag{2}$$

where

$$Y_L = G + j\left(C\omega - \frac{1}{L\omega}\right) \tag{3}$$

is the admittance of the slot resonator, and Y_0 is the reference admittance of the port. Introducing (3) in (2), one obtains

$$\rho = \frac{Y_0 - G - j\left(C\omega - \frac{1}{L\omega}\right)}{Y_0 + G + j\left(C\omega - \frac{1}{L\omega}\right)} \tag{4}$$

and the phase of the reflection coefficient is

$$\phi_\rho = \arctan\left\{\frac{\frac{1}{L\omega} - C\omega}{Y_0 - G}\right\} + \arctan\left\{\frac{\frac{1}{L\omega} - C\omega}{Y_0 + G}\right\}. \tag{5}$$

Thus, the phase slope is

$$\frac{d\phi_\rho}{d\omega} = -\frac{\frac{1}{Y_0 - G}\left(C + \frac{1}{L\omega^2}\right)}{1 + \left[\frac{\frac{1}{L\omega} - C\omega}{Y_0 - G}\right]^2} - \frac{\frac{1}{Y_0 + G}\left(C + \frac{1}{L\omega^2}\right)}{1 + \left[\frac{\frac{1}{L\omega} - C\omega}{Y_0 + G}\right]^2} \tag{6}$$

and evaluation at the resonance frequency gives:

$$\left.\frac{d\phi_\rho}{d\omega}\right|_{\omega_0} = -\frac{4CY_0}{Y_0^2 - G^2} \tag{7}$$

corresponding to the second condition, or equation, of the parameter extraction procedure. Finally, the third condition corresponds to the magnitude of the reflection coefficient at resonance, given by

$$|\rho|_{\omega_0} = \left|\frac{Y_0 - G}{Y_0 + G}\right|. \tag{8}$$

Introducing in (8) the magnitude level of the reflection coefficient at resonance, G is univocally determined. Once G is obtained, expression (7) provides C. Finally, L is obtained from (1). Application of this parameter extraction method to the slot resonator of Fig. 1 has provided the following parameters: L = 2.45 nH, C = 1.15 pF, and G = 1.26 mS. The width of the admittance inverter provides a characteristic impedance of Z_1 = 150 Ω. Note that $G << Y_0 = 1/Z_0 = 20$ mS, as corresponds to the fact that losses are very small. However, this is not necessarily the case when certain MUTs (e.g., liquids) are in contact with the slot resonator, as it will be later shown.

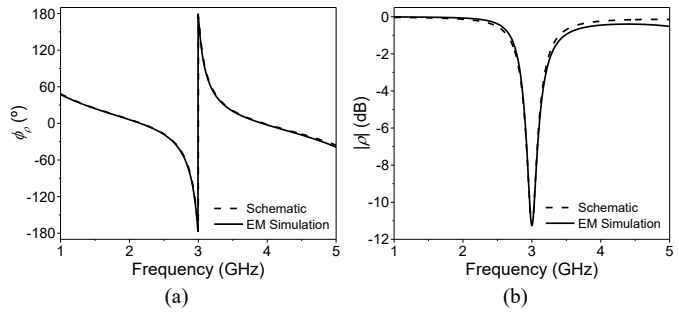

Fig. 2. Frequency response of the structure of Fig. 1(a) obtained by electromagnetic simulation (using *Keysight ADS Momentum*) and circuit simulation. (a) Phase of the reflection coefficient; (b) magnitude of the reflection coefficient.

The circuit response of the structure of Fig. 1 with the extracted parameters, as obtained from the *Keysight ADS* schematic simulator, is also included in Fig. 2 for comparison purposes. The agreement with the electromagnetic simulation is very good, which validates both the circuit model and the parameter extraction procedure.

III. Sensitivity analysis

Let us next assume that a certain material (MUT), either solid or liquid, coats the slot resonator, and that the dielectric properties of such material might be subjected to potential perturbations. Such perturbations can be due to a variation in the composition of the MUT (for example the volume fraction of a certain solution), to a change in the sample, or to a variation in the ambient factors, e.g., temperature and humidity (there are materials with dielectric properties very sensitive to environmental factors). Dielectrically, the MUT is characterized either by the complex permittivity (including the real and the imaginary parts), or by the dielectric constant and loss tangent. In principle, the phase of the reflection coefficient, ϕ_ρ, the considered output variable in this work, might be perturbed by variations in both the dielectric constant, $\varepsilon_{\mathrm{MUT}}$, and the loss tangent, $\tan\delta_{\mathrm{MUT}}$, of the MUT. A variation in $\varepsilon_{\mathrm{MUT}}$ generates a change in the capacitance of the resonator, which in turn alters ϕ_ρ. Such capacitance depends on $\varepsilon_{\mathrm{MUT}}$ (and obviously on the geometry of the slot resonator), but not on $\tan\delta_{\mathrm{MUT}}$. However, the dependence of the conductance on the input variables is more complex. Indeed, the conductance of the resonator loaded with a certain MUT can be expressed as the parallel combination of the conductance of the substrate and the contribution of the MUT (null if the slot resonator is surrounded by air). Let us call the contribution of the conductance of the MUT as G_{MUT}, so that $G = G_{\mathrm{SUBS}} + G_{\mathrm{MUT}}$, where G_{SUBS} is the contribution of the substrate. Of course, any variation in G with regard to the REF value (the one corresponding to the slot resonator loaded with the REF sample) should be entirely due to a variation in G_{MUT}, which can be expressed in terms of the loss tangent as follows [1],[28]

$$G_{MUT} = \tan\delta_{\mathrm{MUT}} \cdot C_{\mathrm{MUT}} \cdot \omega_0 \tag{9}$$

where C_{MUT} is the contribution of the MUT to the slot capacitance, and it depends on $\varepsilon_{\mathrm{MUT}}$ as follows [1],[28]:

$$C_{\mathrm{MUT}} = C_{\mathrm{SUBS}} \cdot \frac{\varepsilon_{\mathrm{MUT}}}{\varepsilon_r} \tag{10}$$

C_{SUBS} being the substrate capacitance. In (9), ω_0 is the angular resonance frequency when the sensor is loaded with the MUT. According to (9) and (10), the conductance of the slot resonator depends on both input variables, $\varepsilon_{\mathrm{MUT}}$ and $\tan\delta_{\mathrm{MUT}}$. It has been assumed in (9) and (10) that the width of the slot resonator is small as compared to the thickness of the substrate and MUT. Under these conditions, the electromagnetic field generated by the slot is circumscribed, to a first order approximation, within the substrate and MUT (semi-infinite approximation), a necessary condition for the validity of (9) and (10). Under such semi-infinite substrate and MUT approximation, there is a quasi-magnetic wall in the plane of the slot resonator (the electric fields in the substrate and MUT are mirror images), and the capacitance of the slot can be expressed as $C_{\mathrm{SUBS}} + C_{\mathrm{MUT}}$, i.e., the sum of the individual contributions of the substrate and MUT to the slot capacitance. As demonstrated in [1], [28], the ratio of these capacitances is proportional to the ratio of dielectric constants of substrate and MUT, from which expression (10) is deduced. The validity of this semi-infinite approximation in the considered prototypes will be discussed later.

According to the previous paragraph, a variation in the phase of the reflection coefficient, $\Delta\phi_\rho$, caused by changes in the input variables, $\Delta\varepsilon_{\mathrm{MUT}}$ and $\Delta\tan\delta_{\mathrm{MUT}}$, should be expressed as follows:

$$\Delta\phi_\rho = \frac{d\phi_\rho}{dC}\cdot\frac{dC}{d\varepsilon_{\mathrm{MUT}}}\cdot\Delta\varepsilon_{\mathrm{MUT}} + \frac{d\phi_\rho}{dG}\cdot\frac{dG}{d\tan\delta_{\mathrm{MUT}}}\cdot\Delta\tan\delta_{\mathrm{MUT}} + \frac{d\phi_\rho}{dG}\cdot\frac{dG}{dC}\cdot\frac{dC}{d\varepsilon_{\mathrm{MUT}}}\cdot\Delta\varepsilon_{\mathrm{MUT}}\,. \tag{11}$$

In (11), two key derivatives (or partial sensitivities) determine the behavior and performance of the proposed sensor, i.e., $d\phi_\rho/dC$ and $d\phi_\rho/dG$. Let us calculate them for the structure of Fig. 1, including the slot resonator and the high-impedance line section. For that purpose, let us designate by C_0 and G_0 the capacitance and conductance, respectively, of the slot resonator loaded with the REF sample. Thus, when a different sample (MUT) is in contact with the slot resonator, it generates potential changes in those elements as $C = C_0 + \Delta C$ and $G = G_0 + \Delta G$. Since C_0 and G_0 are constant, the previous derivatives are identical to $d\phi_\rho/d\Delta C$ and $d\phi_\rho/d\Delta G$. For the calculation of such derivatives, let us first obtain the reflection coefficient seen from the input port (excluding the access line) at the operational frequency, i.e., at the resonance frequency of the slot resonator when it is loaded with the REF sample, $\omega_0 = (LC_0)^{-1/2}$. The calculation is simple since, at that frequency, the high-impedance line section is a quarter-wavelength transmission line, and the admittance seen from the input port is simply

$$Y_{\mathrm{in}} = \frac{Y_1^2}{Y_L}\,. \tag{12}$$

Introducing in (12) the admittance of the slot resonator, as given by (3), with C replaced with $C_0 + \Delta C$, G replaced with $G_0 + \Delta G$, and

ω replaced with ω_0, gives:

$$\rho|_{\omega_0} = \frac{Y_0 - Y_{in}}{Y_0 + Y_{in}} = \frac{jY_0\omega_0\Delta C + Y_0(G_0 + \Delta G) - Y_1^2}{jY_0\omega_0\Delta C + Y_0(G_0 + \Delta G) + Y_1^2} \quad (13)$$

and the phase of the reflection coefficient at the operational frequency is thus:

$$\phi_{\rho,\omega_0} = \arctan\left\{\frac{Y_0\omega_0\Delta C}{Y_0(G_0 + \Delta G) - Y_1^2}\right\} - \arctan\left\{\frac{Y_0\omega_0\Delta C}{Y_0(G_0 + \Delta G) + Y_1^2}\right\}. \quad (14)$$

Using (14), the above-cited derivatives are found to be

$$\frac{d\phi_{\rho,\omega_0}}{d\Delta C} = \frac{\frac{Y_0\omega_0}{Y_0(G_0 + \Delta G) - Y_1^2}}{1 + \left[\frac{Y_0\omega_0\Delta C}{Y_0(G_0 + \Delta G) - Y_1^2}\right]^2} - \frac{\frac{Y_0\omega_0}{Y_0(G_0 + \Delta G) + Y_1^2}}{1 + \left[\frac{Y_0\omega_0\Delta C}{Y_0(G_0 + \Delta G) + Y_1^2}\right]^2} \quad (15)$$

$$\frac{d\phi_{\rho,\omega_0}}{d\Delta G} = -\frac{\frac{Y_0^2\omega_0\Delta C}{(Y_0(G_0 + \Delta G) - Y_1^2)^2}}{1 + \left[\frac{Y_0\omega_0\Delta C}{Y_0(G_0 + \Delta G) - Y_1^2}\right]^2} + \frac{\frac{Y_0^2\omega_0\Delta C}{(Y_0(G_0 + \Delta G) + Y_1^2)^2}}{1 + \left[\frac{Y_0\omega_0\Delta C}{Y_0(G_0 + \Delta G) + Y_1^2}\right]^2}. \quad (16)$$

Let us next assume that the interest is the measurement or detection of small changes in the dielectric properties of the MUT in the vicinity of the REF values (ε_{REF} and $\tan\delta_{REF}$), corresponding to element values $C = C_0$ and $G = G_0$ (or $\Delta C = \Delta G = 0$). Evaluation of the previous derivatives in such limit gives:

$$\left.\frac{d\phi_{\rho,\omega_0}}{d\Delta C}\right|_{\Delta C = \Delta G = 0} = \frac{2\omega_0 Y_0 Y_1^2}{Y_0^2 G_0^2 - Y_1^4} \quad (17)$$

$$\left.\frac{d\phi_{\rho,\omega_0}}{d\Delta G}\right|_{\Delta C = \Delta G = 0} = 0\ . \quad (18)$$

Interpretation of (18) is clear, i.e., at the resonance frequency of the slot resonator loaded with the REF sample, ω_0, in the limit of small perturbations ($\Delta C = \Delta G = 0$), the reflection coefficient is found to be a real number given by

$$\rho|_{\omega_0,\Delta C = \Delta G = 0} = \frac{Y_0 - Y_{in}}{Y_0 + Y_{in}} = \frac{Y_0 G_0 - Y_1^2}{Y_0 G_0 + Y_1^2} \quad (19)$$

and the phase is either ±180º (for $Y_0 G_0 < Y_1^2$) or 0º (for $Y_0 G_0 > Y_1^2$), i.e., constant values. These phase values do not change by varying G, or ΔG, provided the operational frequency is maintained at ω_0, and $\Delta C = 0$, and this explains the null value of the derivative in (18). Thus, if the interest is to optimize the sensitivity in the limit of small perturbations ($\varepsilon_{MUT} \approx \varepsilon_{REF}$ and $\tan\delta_{MUT} \approx \tan\delta_{REF}$), the second and third terms in the right-hand side member of (11) can be ignored, and the sensitivity can be expressed as

$$S|_{\omega_0,\varepsilon_{REF},\tan\delta_{REF}} \equiv \left.\frac{d\phi_\rho}{d\varepsilon_{MUT}}\right|_{\omega_0,\varepsilon_{REF},\tan\delta_{REF}} = \left.\frac{d\phi_{\rho,\omega_0}}{d\Delta C}\right|_{\Delta C = \Delta G = 0} \cdot \left.\frac{d\Delta C}{d\varepsilon_{MUT}}\right|_{\varepsilon_{REF}} \quad (20)$$

where the first term of the product in (20) is (17), and the second term can be easily calculated, since the capacitance, C, of the slot resonator for any arbitrary MUT loading it can be expressed in terms of the capacitance when the load is the REF sample, as follows [1]

$$C = C_0 + \Delta C = C_0\frac{\varepsilon_r + \varepsilon_{MUT}}{\varepsilon_r + \varepsilon_{REF}} \quad (21)$$

and hence

$$\left.\frac{d\Delta C}{d\varepsilon_{MUT}}\right|_{\varepsilon_{REF}} = \frac{C_0}{\varepsilon_r + \varepsilon_{REF}} \quad (22)$$

Thus, introducing (17) and (22) in (20), the following result is obtained

$$S|_{\omega_0,\varepsilon_{REF},\tan\delta_{REF}} = \frac{2\omega_0 Y_0 Y_1^2}{Y_0^2 G_0^2 - Y_1^4} \cdot \frac{C_0}{\varepsilon_r + \varepsilon_{REF}} \quad (23)$$

Note that (21) and (22) are valid by considering the semi-infinite substrate and MUT approximation. Indeed, the consideration of the semi-infinite approximation is not a requirement but simplifies the sensitivity analysis (providing an analytical expression 23). If the MUT is finite, or even a thin-film structure, then the contribution to the sensitivity given by (21) is no longer valid and should be obtained, e.g., numerically, or by means of a dedicated software. Certainly, the sensitivity is degraded if thin-film MUTs are considered, but such reduction in the sensitivity can be compensated, if needed, by cascading further inverter stages (an aspect to be discussed later).

Expression (23) reveals that the sensitivity can be either negative (for $Y_0 G_0 < Y_1^2$) or positive (for $Y_0 G_0 > Y_1^2$). The sensitivity is negative when losses are small ($Y_0 G_0 < Y_1^2$). In the limit when losses can be neglected (low loss MUTs), $G_0 = 0$ (or $\tan\delta_{REF} = 0$), and the sensitivity is found to be

$$S|_{\omega_0,\varepsilon_{REF},\tan\delta_{REF}=0} = \frac{-2\omega_0 Y_0 C_0}{Y_1^2(\varepsilon_r + \varepsilon_{REF})} = \frac{-2\omega_0 Z_1^2 C_0}{Z_0(\varepsilon_r + \varepsilon_{REF})} \quad (24)$$

According to (24), the presence of the high impedance line, with impedance Z_1, contributes to enhance the sensitivity. From this result, it can be concluded that if losses are negligible, the strategy to boost up the sensitivity is to cascade a quarter-wavelength transmission line with the highest possible characteristic impedance to the slot resonator. However if losses cannot be neglected but satisfy $Y_0 G_0 < Y_1^2$, in that case, the strategy to boost up the sensitivity is to choose the admittance of the quarter-wavelength admittance inverter Y_1 slightly superior to

$\sqrt{Y_0 G_0}$, so that the denominator in (23) is a negative number close to zero.

If losses are important ($Y_0 G_0 > Y_1^2$), a possible situation when dealing with liquid samples, the strategy to boost up the sensitivity is to set Y_1 to a value slightly inferior to $\sqrt{Y_0 G_0}$. It should be mentioned that the operational regime of the sensor (either low-loss or high-loss) is not something inherent to the level of losses of the MUT. The reason is that the condition that separates both regimes ($Y_0 G_0 = Y_1^2$) depends on a sensor design parameter, i.e., Y_1. In other words, depending on the level of losses of the MUT, and hence G_0, it might be possible to tailor Y_1 in order to force the sensor to operate either under the low-loss regime ($Y_0 G_0 < Y_1^2$) or under the high-loss regime ($Y_0 G_0 > Y_1^2$). However, an important aspect to take into account is that a change of regime within the considered input dynamic range of the sensor should be avoided, as it generates a sudden change in the phase of the reflection coefficient, due to the change of the sign in the sensitivity. It must also be indicated that the condition that separates the low-loss and the high-loss regime ($Y_0 G_0 = Y_1^2$) is valid for the structure of Fig. 1, with a single admittance inverter (with admittance Y_1). The boundary between both regimes changes when additional quarter-wavelength admittance inverters with alternating low/high impedance are cascaded to the one of Fig. 1, an aspect to be discussed next.

The generalization of the sensitivity given by (23) to the case where the sensor is implemented with N inverters (see Fig. 3) is relatively simple. The admittance seen from the input port (excluding the access line) can be expressed as

$$Y_{\text{in},N} = Y_L^{(-1)^N} \cdot \prod_{i=1}^{N} Y_i^{2(-1)^{i+N}} \tag{25}$$

where Y_i is the admittance of inverter i. For N odd, the reflection coefficient evaluated at ω_0 is

$$\rho|_{\omega_0} = \frac{Y_0 - Y_{\text{in},N}}{Y_0 + Y_{\text{in},N}} = \frac{jY_0\omega_0\Delta C + Y_0(G_0 + \Delta G) - \prod_{i=1}^{N} Y_i^{2(-1)^{i+N}}}{jY_0\omega_0\Delta C + Y_0(G_0 + \Delta G) + \prod_{i=1}^{N} Y_i^{2(-1)^{i+N}}} \tag{26}$$

and the sensitivity in the limit of small perturbations is found to be

$$S|_{\omega_0,\varepsilon_{\text{REF}},\tan\delta_{\text{REF}}} = \frac{2\omega_0 Y_0 \cdot \prod_{i=1}^{N} Y_i^{2(-1)^{i+N}}}{Y_0^2 G_0^2 - \left(\prod_{i=1}^{N} Y_i^{2(-1)^{i+N}}\right)^2} \cdot \frac{C_0}{\varepsilon_r + \varepsilon_{\text{REF}}} \,. \tag{27}$$

For N even, the reflection coefficient evaluated at ω_0 is

$$\rho|_{\omega_0} = \frac{Y_0 - Y_{\text{in},N}}{Y_0 + Y_{\text{in},N}} = \frac{Y_0 - (G_0 + \Delta G + j\omega_0\Delta C) \cdot \prod_{i=1}^{N} Y_i^{2(-1)^{i+N}}}{Y_0 + (G_0 + \Delta G + j\omega_0\Delta C) \cdot \prod_{i=1}^{N} Y_i^{2(-1)^{i+N}}} \tag{28}$$

and the sensitivity in the limit of small perturbations is

$$S|_{\omega_0,\varepsilon_{\text{REF}},\tan\delta_{\text{REF}}} = \frac{-2\omega_0 Y_0 \cdot \prod_{i=1}^{N} Y_i^{2(-1)^{i+N}}}{Y_0^2 - G_0^2 \left(\prod_{i=1}^{N} Y_i^{2(-1)^{i+N}}\right)^2} \frac{C_0}{\varepsilon_r + \varepsilon_{\text{REF}}} \,. \tag{29}$$

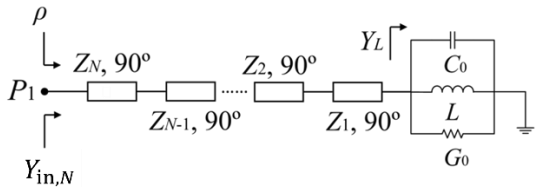

Fig. 3. Schematic of the generalized sensor with an arbitrary number, N, of inverters.

As it can be seen from (27) and (29), the boundary between the low-loss and the high-loss regime depends on the number of quarter-wavelength impedance inverters, N, and the specific expression is different for N even and for N odd. Let us summarize next:

- For N odd, the low-loss regime requires that

$$Y_0 G_0 < \prod_{i=1}^{N} Y_i^{2(-1)^{i+N}} \tag{30}$$

and this condition becomes more restrictive as the number of stages increases. For instance, for $N = 1$, the case studied in detail before, the condition is $Y_0 G_0 < Y_1^2$, whereas for $N = 3$, the low-loss regime requires that $Y_0 G_0 < Y_1^2 Y_3^2 / Y_2^2$, namely a significantly smaller value of G_0 is needed, since $Y_1 < Y_0$, $Y_3 < Y_0$, and $Y_2 > Y_0$, as dictated by sensitivity optimization requirements in the low loss regime.
- For N even, the condition for operation under the low-loss regime is

$$G_0 \cdot \prod_{i=1}^{N} Y_i^{2(-1)^{i+N}} < Y_0 \tag{31}$$

and for operation under this regime, the value of G_0 must decrease as the number of stages, N, increases. For example, for $N = 0$ (corresponding to the absence of inverters), the condition (31) is $G_0 < Y_0$; for $N = 2$, the low-loss regime requires that $G_0 Y_2^2 / Y_1^2 < Y_0$ (or $G_0 < Y_0 Y_1^2 / Y_2^2$), i.e., much more restrictive for G_0, provided $Y_1 < Y_0 < Y_2$.

As for the case with $N = 1$, if losses are negligible, to boost up the sensitivity in the limit of small perturbations, it is necessary to set the admittance of the line section adjacent to the resonator to a small value (high value of Z_1). The further cascaded sections (if they are present) must then alternate the impedance value, with Z_2 low, Z_3 high, and so on. However, if losses are not negligible, regardless on the specific operation regime (low-loss or high-loss), it is possible to control (enhance) the sensitivity in the limit of small perturbations. For that purpose, the impedance values of the inverter stages should be adjusted, so that the denominator in (27) or (29) is made small (corresponding to sensor operation near the boundary between both regimes).

It is interesting to mention that the sensitivity is negative for

low losses, whereas it is positive under the high-loss sensor operation regime [see expressions (27) and (29)]. The sign of the sensitivity is intimately related to the phase slope of the reflection coefficient at the operating frequency. It is well-known that the phase slope when losses are absent should always be negative. A negative phase slope means that when the dielectric constant of the MUT increases, the phase shifts downwards. Consequently, the phase at the (fixed) operational frequency decreases, and hence the sensitivity is negative. According to this argument, it follows that a positive phase slope should correlate with a positive sensitivity. Nevertheless, to gain insight on this aspect, let us calculate next the phase slope for the structure of Fig. 1 in the vicinity of resonance, when the sensor is loaded with the REF sample (providing a slot capacitance and conductance of C_0 and G_0, respectively). Since the objective is to calculate the phase slope near resonance, where the line cascaded to the slot resonator exhibits an electrical length of 90º, it is reasonable to assume that such line behaves as an ideal inverter, with input impedance given by (12). The reflection coefficient can be expressed as

$$\rho = \frac{Y_0 G_0 - Y_1^2 + jY_0\left(C_0\omega - \frac{1}{L\omega}\right)}{Y_0 G_0 + Y_1^2 + jY_0\left(C_0\omega - \frac{1}{L\omega}\right)} \quad . \tag{32}$$

Thus, the phase of the reflection coefficient is

$$\phi_\rho = \arctan\left\{\frac{Y_0\left(C_0\omega - \frac{1}{L\omega}\right)}{Y_0 G_0 - Y_1^2}\right\} - \arctan\left\{\frac{Y_0\left(C_0\omega - \frac{1}{L\omega}\right)}{Y_0 G_0 + Y_1^2}\right\} \tag{33}$$

and the phase slope is

$$\frac{d\phi_\rho}{d\omega} = -\frac{\frac{Y_0}{Y_0 G_0 - Y_1^2}\left(C_0 + \frac{1}{L\omega^2}\right)}{1 + \left[\frac{Y_0\left(C_0\omega - \frac{1}{L\omega}\right)}{Y_0 G_0 - Y_1^2}\right]^2} - \frac{\frac{Y_0}{Y_0 G_0 + Y_1^2}\left(C_0 + \frac{1}{L\omega^2}\right)}{1 + \left[\frac{Y_0\left(C_0\omega - \frac{1}{L\omega}\right)}{Y_0 G_0 + Y_1^2}\right]^2} \tag{34}$$

Evaluation of (34) at the resonance frequency, $\omega_0 = (LC_0)^{-1/2}$, gives

$$\left.\frac{d\phi_\rho}{d\omega}\right|_{\omega_0} = \frac{4Y_0 C_0 Y_1^2}{Y_0^2 G_0^2 - Y_1^4} \tag{35}$$

namely, the phase slope is negative as far as losses satisfy $Y_0 G_0 < Y_1^2$. Note that this condition (low loss regime) is the one required to obtain a negative sensitivity [see expression (23)]. The generalization of this study for an arbitrary number of inverters, N, not included in the paper, reveals that the phase slope at resonance is negative provided expressions (30), for N odd, or (31), for N even, are satisfied (corresponding to the low-loss regime).

Let us next validate the previous analysis on the phase slope at resonance through full-wave electromagnetic simulation and circuit simulation with parameter extraction. For that purpose, let us consider the structure of Fig. 1 loaded with two hypothetical REF materials. The considered dielectric constant in both cases is $\varepsilon_{REF} = 3.6$, whereas the loss tangent is $\tan\delta_{REF,1} = 0.002$ for material 1 (low-loss sample) and $\tan\delta_{REF,2} = 0.08$ for material 2 (high-loss sample). Both materials are semi-infinite in the vertical direction. The simulated phase responses of both structures are depicted in Fig. 4. It should be clarified that with the introduction of a MUT on top of the slot, it has been imperative to resize the length of the admittance inverter (now being $l_i = 20.2$ mm) in order to achieve an electrical length of 90º at $f_0 = 2.33$ GHz (the resonance frequency of the slot loaded with the hypothetical REF materials). As it can be seen, for sample 1, the phase experiences a jump at resonance, i.e., $\phi_\rho = \pm 180º$, whereas the phase is $\phi_\rho = 0º$ at that frequency for sample 2. Parameter extraction has provided the following reactive parameter values for both samples: $L = 2.45$ nH, $C_0 = 1.86$ pF. The resulting conductance is $G_0 = 1.05$ mS for sample 1 and $G_0 = 2.32$ mS for sample 2. The circuit responses are also included in Fig. 4, and the agreement with the electromagnetic simulation is excellent. For the low-loss sample (material 1), $Y_0 G_0 < Y_1^2$, (being $Y_1 = 6.67$ mS) and the reflection coefficient (32) is a negative real number at resonance. Thus, the phase at that frequency is $\phi_\rho = \pm 180º$. By contrast, for material 2 (high-loss sample), $Y_0 G_0 > Y_1^2$, and the reflection coefficient is a positive real number at resonance. Consequently, the phase of the reflection coefficient at resonance is $\phi_\rho = 0º$, as it can be appreciated in Fig. 4.

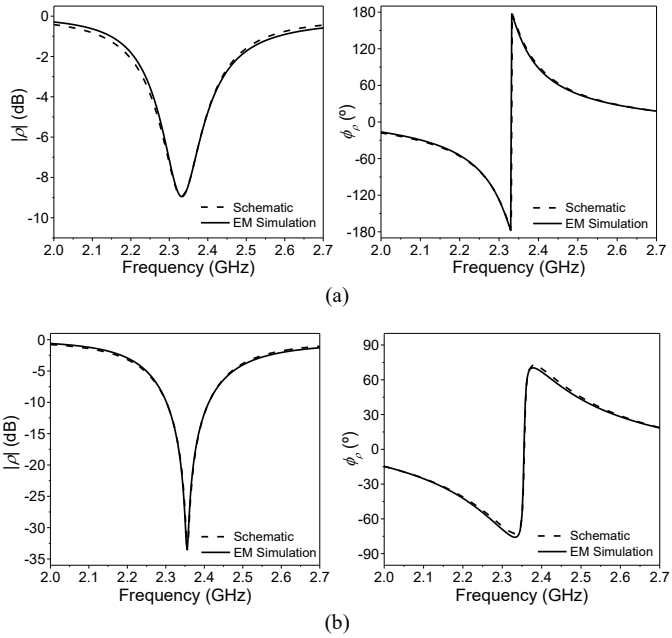

Fig. 4. Electromagnetic and circuit simulation of the frequency response (magnitude and phase) of the structure of Fig. 1(a) when the slot resonator is loaded with the hypothetical materials 1 and 2 with dielectric characteristics indicated in the text. (a) Magnitude and phase response for material 1; (b) magnitude and phase response for material 2.

To demonstrate that the operational regime of the sensor might depend also on the number of inverters, we have simulated the previous structures (by considering materials 1 and 2), but eliminating the inverter ($N = 0$), see Fig. 5. In this case, the limit between the low-loss and the high-loss regime is less restrictive, i.e., $G_0 < Y_0$ suffices to be under the low-loss

condition. Since G_0 satisfies the previous condition for both REF materials, in this case ($N = 0$), the structure operates under the low-loss regime for both materials, the phase slope is negative, and the phase value at resonance is $\phi_\rho = 0^\text{o}$, identical to the lossless case without admittance inverters. Note that for the lossless case, an open provides a null in the phase of the reflection coefficient, and such phase prevails at resonance as far as $G_0 < Y_0$, since under this condition the reflection coefficient at resonance is a positive real number [see expression (4)].

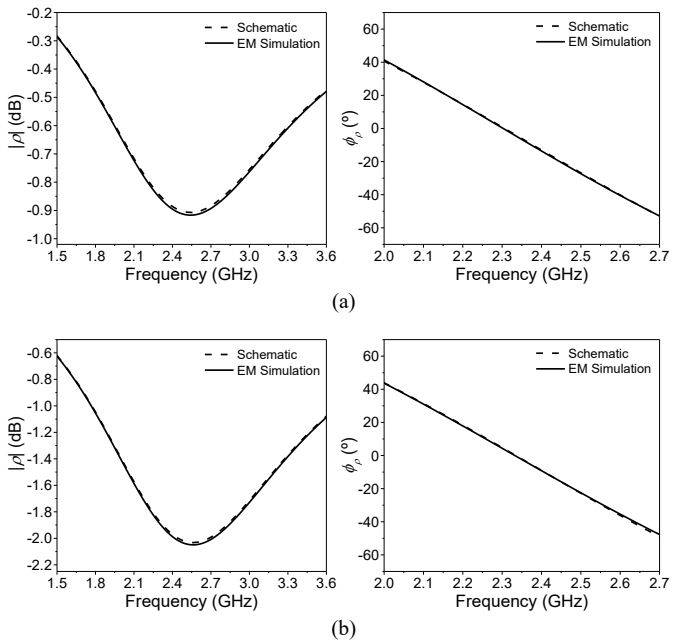

Fig. 5. Electromagnetic and circuit simulation of the frequency response (magnitude and phase) of the structure of Fig. 1(a) without the admittance inverter, when the slot resonator is loaded with the hypothetical materials 1 and 2 with dielectric characteristics indicated in the text. (a) Magnitude and phase response for material 1; (b) magnitude and phase response for material 2.

Let us next investigate a case with $N = 2$. For that purpose, we have considered the sensor of Fig. 1, with an additional (cascaded) low-impedance quarter-wavelength transmission line. The characteristic admittance of such line is $Y_2 = 0.033$ S. Note that, in this case, operation under the low-loss regime requires that $G_0 Y_2^2 / Y_1^2 < Y_0$ (or $G_0 < Y_0 Y_1^2 / Y_2^2$), see (31), i.e., a very restrictive condition, as far as $Y_1 < Y_0 < Y_2$. The values of G_0 for both REF materials are not small enough to satisfy the previous low-loss operation condition. Consequently, in this case, operation proceeds under the high-loss regime, and the phase slope at resonance is positive for both REF materials, see Fig. 6. With $N = 2$, the phase of the reflection coefficient at resonance for the lossless case, or for the low-loss operation regime, should be $\phi_\rho = 0^\text{o}$. Note however, that the phase obtained from both circuit and electromagnetic simulation experiences a jump ($\phi_\rho = \pm 180^\text{o}$) at resonance for both materials, indicative of operation under the high-loss regime.

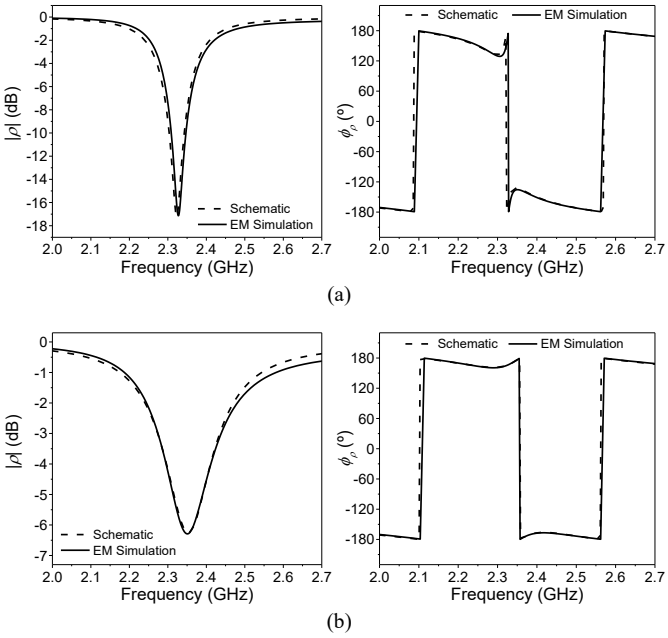

Fig. 6. Electromagnetic and circuit simulation of the frequency response (magnitude and phase) of the structure of Fig. 1(a) with an additional quarter-wavelength transmission line with characteristic impedance $Z_2 = 1/Y_2 = 30\ \Omega$, when the slot resonator is loaded with the hypothetical materials 1 and 2 with dielectric characteristics indicated in the text. (a) Magnitude and phase response for material 1; (b) magnitude and phase response for material 2.

The results of Figs. 4, 5 and 6 point out the importance of the number of stages (N) on sensor behavior, and are indicative of the intimate link between the phase slope at resonance and sensitivity. Let us next experimentally validate the proposed sensors, by considering both solid and liquid samples. Nevertheless, let us first mention that in Figs. 4 and 6, the notch in the magnitude of the reflection coefficient is significant (contrary to Fig. 5). The notch is caused by losses, and such losses can be due to material losses (dielectric and ohmic) or radiation losses. When the slot is directly connected to the access line (without inverters, or $N = 0$), the case of Fig. 5, the notch is soft and can be caused in part by absorption or by radiation, though the soft notch indicates that radiation should not be significant. When the inverters are added, case of Figs. 4 and 6, what happens is that the inverters transform the conductance G_0 at resonance to a value closer to the reference conductance of the port, and the reflection coefficient dramatically decreases (or the notch depth in dB increases).

IV. Sensor Validation

For experimental validation of the sensors proposed in this paper, we have considered the structure of Fig. 1, with $N = 1$, and we have applied it to the characterization of solid and liquid samples. Nevertheless, a redesign has been made in each case, in order to optimize the sensitivity. Concerning solids, the considered samples are low-loss dielectric slabs, corresponding in most cases to uncladded microwave substrates available in our laboratory. Actually, we have stacked several samples in order to ensure a sufficient MUT thickness to guarantee the semi-infinite approximation. This is not necessary for sensor functionality, but to compare the resulting sensitivity with the

analytical predictions (where such approximation has been adopted). The REF sample is the uncladded *Rogers 4003C* substrate with dielectric constant ε_{REF} = 3.55 and loss tangent $\tan\delta_{REF}$ = 0.0022. Concerning the characterization of liquid samples, in this paper the interest is the characterization of the volume fraction of isopropanol in diluted solutions of deionized (DI) water. Therefore, the REF sample is pure DI water, with dielectric constant ε_{REF} = 78.70 and loss tangent $\tan\delta_{REF}$ = 0.049 at 1 GHz and room temperature (23ºC). Let us mention that the sensor devoted to solid samples operates under the low-loss regime, whereas the liquid sensor works under the high-loss regime, as it will be shown. Let us next discuss separately the details associated to both sensors.

A. Sensor for Solids. Operation Under the Low-loss Regime

For sensitivity optimization in the limit of small perturbations when very low-loss samples are considered ($Y_0 G_0 \ll Y_1^2$), expression (23) [or the resulting expression with negligible losses (24)] reveals that Y_1 must be small (corresponding to a high impedance quarter-wavelength line section) and C_0 must be high. Since the operational frequency should be set to a certain value, i.e., the resonance frequency of the slot resonator loaded with the REF sample ($f_0 = \omega_0/2\pi$ = 2.36 GHz in the present sensor), an increase in C_0 is necessarily associated to a decrease in L. Therefore, for sensitivity optimization in the limit of small perturbations, a high-Q resonator is needed. In order to increase the capacitance of the slot with a small value of the inductance, the strategy has been to reduce the slot width to the minimum possible value dictated by the available fabrication technology (0.2 mm in our case). The impedance of the quarter-wavelength (at f_0) line section has been set to Z_1 = 150 Ω (or Y_1 = 6.67 mS).

Sensor implementation has been carried out on the *Rogers 4003C* commercial microwave substrate, with dielectric constant ε_r = 3.55, thickness h = 1.524 mm and loss factor tanδ = 0.0022. The photograph of the fabricated device, including the 50-Ω access line, is depicted in Fig. 7, where dimensions are indicated. Note that, rather than a grounding via, the slot resonator has been connected to ground by means of an open-ended quarter-wavelength (90º) transmission line with impedance Z_1 (which provides a virtual ground at the plane of the resonator at f_0). Figure 8 depicts the frequency response (reflection coefficient, or S_{11}), including the magnitude and the phase, by considering that the slot resonator is covered with the REF material, as obtained from full-wave electromagnetic simulation and measurement. The measurements have been obtained by means of the *Agilent N5221A* vector network analyzer, whereas the simulation has been obtained by means of the *Ansys HFSS* commercial full-wave simulator. The parameters of the slot resonator (covered with the REF sample) have been extracted from the simulated response, and the circuit response, also included in Fig. 8, is in very good agreement with the simulations and measurements (the extracted parameters are L = 2.76 nH, C_0 = 1.64 pF and G_0 = 1.1 mS).

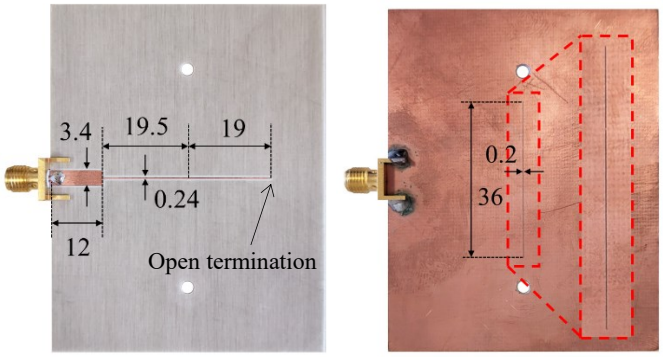

Fig. 7. Photograph of the slot-based sensor devoted to the characterization of solid samples (a) Top view; (b) bottom view. Dimensions are given in mm. Note that the lengths of the quarter-wavelength lines (the one between the access line and the slot, 19.5 mm, and the one replacing the via, 19.0 mm) are slightly different to account for the fringing field effects of the open end. Both line sections exhibit an electrical length of 90º.

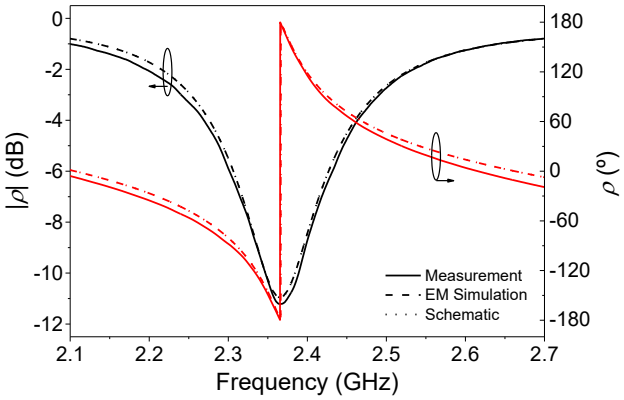

Fig. 8. Frequency response of the fabricated sensor of Fig. 7, when it is loaded with the REF sample.

Next, we have experimentally obtained the phase response of the reflection coefficient for different samples (i.e. air, polylactic acid –*PLA*–, and *FR4*). The results are depicted in Fig. 9(a), where they are compared with the simulated values. Fig. 9(b) includes the phase of the reflection coefficient at f_0 and the sensitivity as deduced from the simulated data points (note that the sensitivity cannot be easily retrieved from the experimental data due to the lack of a significant number of data points). The sensitivity in the limit of small perturbations that results from the simulated data is S_{sim} = –255.5º, whereas the theoretical prediction given by (23) provides S_{th} = –234,05º. This slight discrepancy is due to the fact that the substrate (with a thickness of h = 1.524 mm) cannot be actually considered to be semi-infinite, an assumption made for the calculation of the sensitivity. However, if we replace ε_r in (23) with $\varepsilon_{r,eq}$, the so-called equivalent dielectric constant of the substrate, then the theoretical sensitivity is found to be S_{th} = –253.89º), in very good agreement with the simulated value. The equivalent dielectric constant of the substrate, defined as the dielectric constant of a hypothetical semi-infinite substrate providing the same contribution to the capacitance of the slot, has been found to be $\varepsilon_{r,eq}$ = 3.20 (the procedure to calculate it can be found in [59]).

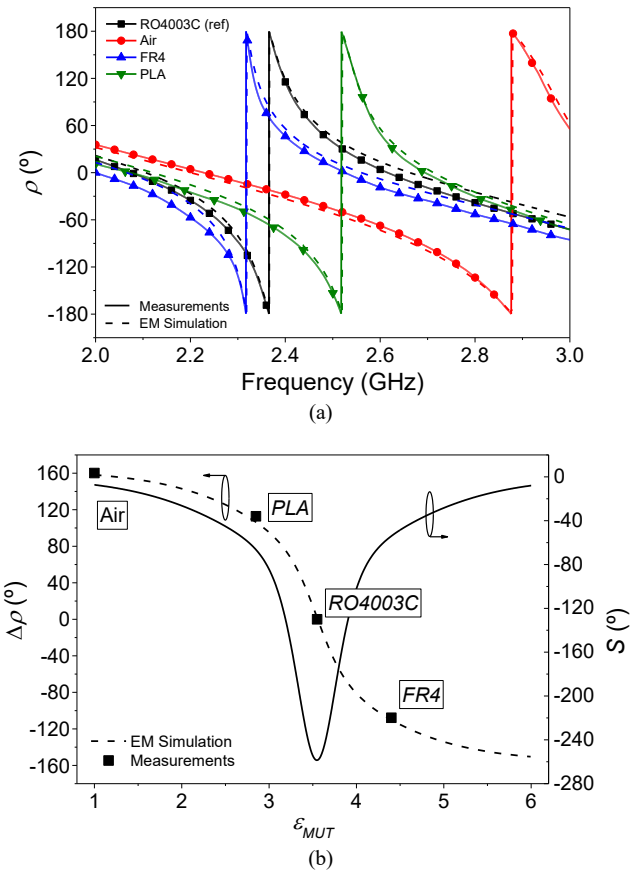

Fig. 9. Simulated and measured phase response of the reflection coefficient for the sensor of Fig. 7 with different samples (a) and dependence of the phase of the reflection coefficient at the operating frequency with the dielectric constant of the MUT and sensitivity as deduced form the simulated data points (b). The samples were pressed against the sensor to minimize the effects of the air gap layer.

B. Sensor for Liquids. Operation Under the High-Loss Regime

The main difference of the sensor devoted to liquids, as compared to the one of the previous subsection, is the fact that it operates under the high-loss regime. The considered REF liquid is DI water, and the main objective of the proposed sensor is to detect the presence of very small volume fractions of isopropanol in DI water (for this reason we have considered pure DI water as REF material). In order to put in contact the liquid sample with the sensing element, i.e., the slot resonator, a holder (container) made of polylactic acid (PLA) has been 3D-printed by means of the *Ultimaker 3 Extended* 3D printer. The height of the holder (10 mm) is enough to guarantee that the MUT liquid is semi-infinite in the vertical direction. The photograph of the fabricated sensor is depicted in Fig. 10, where dimensions are indicated. Like the sensor for solids of Fig. 7, the grounding via has been replaced with an open-ended 90º transmission line. The high-impedance quarter-wavelength transmission line cascaded to the slot resonator exhibits a characteristic impedance of $Z_1 = Y_1^{-1} = 107\ \Omega$. The sensor has been implemented in the *Rogers 4003C* substrate with dielectric constant $\varepsilon_r = 3.55$, thickness $h = 1.524$ mm, and loss factor $\tan\delta = 0.0022$. To avoid liquid absorption by the substrate, a 50-μm thick *SU-8* dry film with an estimated dielectric constant of $\varepsilon_{r,\text{film}} = 3.1$ and loss factor of $\tan\delta_{\text{film}} = 0.053$ has been used.

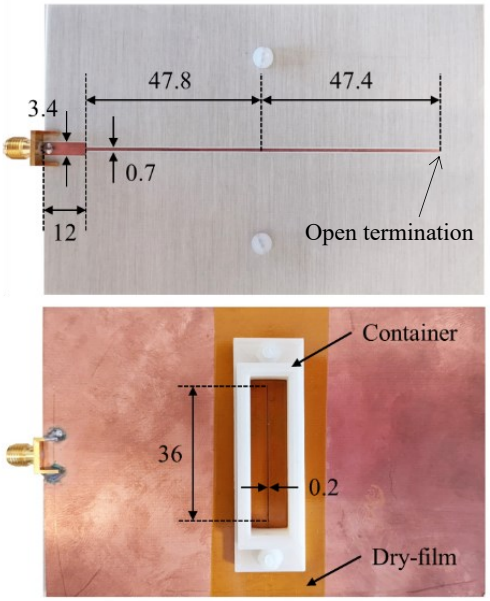

Fig. 10. Photograph of the slot-based sensor devoted to the characterization of liquid samples (top view upper and bottom view lower). Dimensions are given in mm. Note that the lengths of the quarter-wavelength lines (the one between the access line and the slot, 47.8 mm, and the one replacing the via, 47.4 mm) are slightly different to account for the fringing field effects of the open end.

We have extracted the parameters of the slot resonator with the presence of DI water on top of it, and the resulting values are $L = 2.00$ nH, $C_0 = 12.76$ pF, and $G_0 = 4.7$ mS. Since G_0 is relatively high, the sensor has been designed to operate in the high-loss regime. Nevertheless, the admittance of the quarter-wavelength transmission line, Y_1, has been adjusted in order to obtain a positive value of $Y_0^2 G_0^2 - Y_1^4$, but close to zero, since this term appears in the denominator of the sensitivity (23). This justifies the value of Y_1 (or Z_1) indicated above. The frequency response of the structure (phase and magnitude) when it is loaded with the REF sample (DI water) is depicted in Fig. 11. Very good agreement between the measured response and those obtained by electromagnetic and circuit simulation can be appreciated.

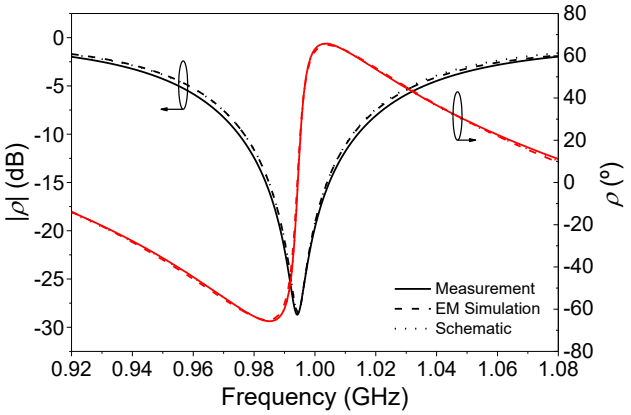

Fig. 11. Frequency response of the fabricated sensor of Fig. 10, when it is loaded with the REF sample (DI water).

Next, we have experimentally obtained the phase response of the reflection coefficient for the different samples, consisting of mixtures of DI water with different percentages (volume fractions) of isopropanol (homogeneous solutions were achieved by mixing the samples using a using a vortex mixer, i.e. *Lab Dancer*, during 120 s for each sample). The different mixtures of DI water and isopropanol, with a total volume of 3 mL, have been introduced in the container by means of a syringe. These mixtures encompass volume fractions ranging from 0% (pure DI water) to 30% of isopropanol. The results are depicted in Fig. 12(a). The figure also includes the phase of the reflection coefficient for the different samples at the operating frequency (f_0 = 0.995 GHz) and the sensitivity as deduced from the measured data points [Fig. 12(b)]. We have opted in this work to consider the same dimensions of the sensing slot for both the sensor of Fig. 10 (dedicated to liquids) and the one of Fig. 7 (devoted to solids). Since the REF material in the sensor of Fig. 10 is DI water, with very high dielectric constant, the resonance frequency in that sensor is much smaller as compared to that of Fig. 7.

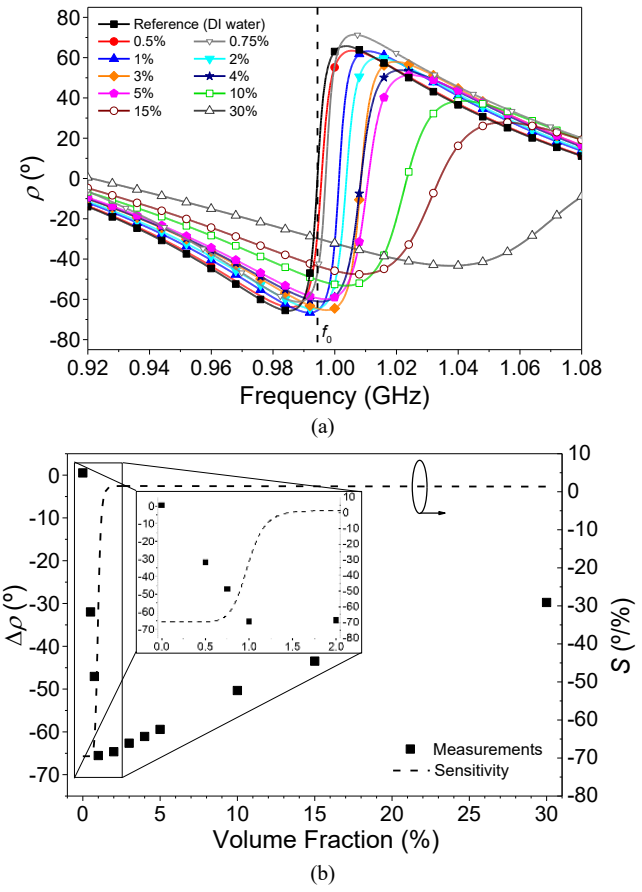

Fig. 12. Measured phase response of the reflection coefficient for the sensor of Fig. 10 with different mixtures of isopropanol in DI water (a), and dependence of the phase of the reflection coefficient at f_0 with the volume fraction of isopropanol and sensitivity (b). Measurements were made at room temperature (23ºC).

The sensitivity in the limit of small perturbations (very small isopropanol concentration) has been found to be 64.96 °/%. Since the isopropanol content correlates with the dielectric constant of the mixture, we have conducted simulations to estimate the dielectric constant of the solution with 0.5% volume fraction of isopropanol in DI water. This allows us to map the sensitivity with volume fraction variation to that with dielectric constant variation, as given by expression (23). The simulated results indicate that the dielectric constant for the indicated volume fraction is ε_{MUT} (0.5%) = 78.49. This variation in the dielectric constant as compared to the one of pure DI water ($\Delta\varepsilon_r$ = 0.21), leads to a sensitivity of S_{meas} = 154.6º, whereas the theoretical prediction given by (23) provides S_{th} = 155.4º, i.e., in very good agreement.

Note that, according to Fig. 12(b), the sensitivity with volume fraction variations in the limit of small perturbations is negative, rather than positive, even though the sensor operates in the high-loss regime. The reason is that, as the volume fraction of isopropanol increases, the dielectric constant of the solution, ε_{MUT}, decreases. Thus, the sensitivity with dielectric constant variations in the limit of small perturbations is positive, as expected. Also note that for volume fractions above 1%, the sensor exhibits a different behavior, with positive (and much smaller) sensitivity with volume fraction variation. This behavior is due to the extremely high sensitivity of the sensor in the limit of small perturbations (visible by the high slope in the phase response), which saturates the response at f_0 for a volume fraction of roughly 1%. Thus, the proposed sensor is mainly useful for detecting very tiny variations of volume fraction of isopropanol in the vicinity of the REF value (0%), and the achieved (measured) sensitivity in the limit of small perturbations agrees with the theoretical prediction, as demonstrated in the preceding paragraph. Nevertheless, the fact that the sensitivity is roughly constant for volume fractions above 1% makes the device also useful in applications where the input dynamic range should encompass large volume fractions (note the good linearity up to volume fractions of 30%).

V. Comparative Analysis and Discussion

As pointed out in the introduction section, various types of reflective-mode phase-variation permittivity sensors have been recently reported. Probably, the most distinctive feature of the sensors reported in this paper is the use of a slot resonator as sensing element. Since such slot is etched in the ground plane of the microstrip-line based sensor structure, the MUT, either solid or liquid, and eventually any additional required mechanical accessory (e.g., the liquid holder), are isolated from the microwave circuitry (the impedance inverters). By contrast, in other reflective-mode phase-variation sensors, the sensing element is a metallic resonator, either distributed [3],[13],[19], or semi-lumped [16],[20]. The sensor reported in [15], based on an open complementary split ring resonator (OCSRR), is an exception, since the OCSRR is an electrically small planar component that can be categorized as a slot-type resonator. However, in such sensor, the sensing OCSRR is the termination of a coplanar waveguide (CPW) transmission line structure. Therefore, the backside isolation capability of the sensors

reported in this paper is not present in those OCSRR-based sensors.

Another interesting aspect of the sensors of this work is the small size of the sensing region. It suffices to extend it transversally a few millimeters beyond the cross-section of the slot resonator to guarantee that the fields generated in the slot do not reach the MUT boundaries. Such small size of the sensing region, A_s, and the high achieved maximum sensitivity, S_{max}, provide a good relation between the maximum sensitivity and the size of the sensing region expressed in terms of the squared guided wavelength, λ^2, for both prototypes. This is the main considered figure of merit (FoM) in reflective-mode phase-variation sensors. Nevertheless, it should be mentioned that the sensitivity in the sensors presented in this work depends inversely on $\varepsilon_r + \varepsilon_{REF}$, see (23), (27) and (29). Thus, the maximum sensitivity in the second prototype (the liquid sensor), $S_{max} = 154.6º$, is moderate as compared to those of other similar sensors because the REF liquid is DI water, with very high dielectric constant, $\varepsilon_{REF} = 78.7$. Such dependence, or a similar dependence (particularly, on the inverse of the effective dielectric constant) is also encountered in other reflective-mode phase-variation sensors. Consequently, for a faithful comparison with other reflective-mode phase-variation sensors devoted to solids samples, with REF dielectric constants typically below 10 (i.e., $\varepsilon_{REF} < 10$), we should consider the product FoM·ε_{REF} as the most representative comparison factor and indicator of sensor performance. For the prototype liquid sensor reported in Section IV.B (Fig. 10), such factor is FoM·ε_{REF} = 608351º/λ^2, the highest in Table I. Such table summarizes the performance and relevant characteristics of various phase-variation permittivity sensors, including not only those sensors operating in reflection, but also those based on transmission-mode structures. In some cases [4],[7],[8], the working principle is phase variation, but the output variable is a magnitude (of the transmission or cross-mode transmission coefficient). Hence, for such sensors, the FoM and the above-cited performance indicator, FoM·ε_{REF}, are not provided.

In view of Table I, the prototype of Fig. 10, operating in the high-loss regime and with the impedance of the inverter calculated to achieve a high sensitivity, is very competitive. Such sensor, and the one reported in [58] (from which this work has been extended), are the first reported prototypes of reflective-mode phase-variation liquid sensors based on an impedance inverter terminated with a slot (sensing) resonator.

TABLE I
COMPARISON OF VARIOUS PHASE-VARIATION SENSORS

Ref.	Operational mode*	f_0 (GHz)	A_S (λ^2)	$\lvert S_{max}\rvert$	FoM (º/λ^2)	FoM·ε_{REF} (º/λ^2)
[3]	RX	2.0	0.025	528.7º	21148	21148
[13]	RX	2.0	0.100	45.5º	455	455
[4]	TX	2.3	---	600 dB	---	---
[5]	TX	---	---	54.8º	---	---
[6]	TX	6.0	12.90	415.6º	32.2	114
[7]	TX	---	0.075	25.3 dB	---	---
[8]	TX	2.0	0.020	17.6 dB	---	---
[10]	TX	2.0	0.040	20.0º	500	500
[15]	RX	2.0	0.015	83.35º	5643	5643
[16]	RX	2.0	0.018	66.5º	3643	12932
[20]	RX	2.0	0.017	468º	27419	27419
[19]	RX	3.45	0.070	659.6º	9401	33373
Fig. 7	**RX**	**2.36**	**0.021**	**255.5º**	**12166**	**43189**
Fig. 10	**RX**	**0.995**	**0.020**	**154.6º**	**7730**	**608351**

*RX: reflection mode; TX: transmission mode.

To end this section, let us mention that although the output variable in the considered sensors is the phase of the reflection coefficient at the operating frequency, by also considering the magnitude of the notch, related to losses, the complex permittivity of the MUT (or the loss tangent) might be obtained. Nevertheless, we do consider that there are other methods which provide more accuracy for the determination of the loss tangent (in particular, sensors based on resonant cavities, see [1] and references therein). For this main reason, this aspect (retrieving the loss tangent) is out of the scope in this paper. Nevertheless, there are many variables intimately related to the dielectric constant, e.g., liquid composition, the case of the proposed liquid sensor, or physical variables, such as temperature or humidity, that can be measured with the proposed sensors (in this regard, functional films exhibiting a high sensitivity of the dielectric constant with those physical variables are convenient). Thus, the applications of the sensors proposed in this work can be diverse, i.e., not only devoted to dielectric constant measurements or material composition. In certain applications, linearity might be more important than achieving a high sensitivity in the vicinity of a REF dielectric constant. Sacrificing sensitivity in favor of linearity can be achieved by degrading the quality factor of the slot resonator and by directly driving it with the access line (i.e., without the presence of impedance inverters, or $N = 0$).

VI. CONCLUSION

In conclusion, a new reflective-mode phase-variation permittivity sensor implemented in microstrip technology and based on a cascade of high/low impedance inverters terminated with a slot resonator has been presented, analyzed, and experimentally validated. The main novel aspect of the paper concerns the fact that, for the first time, the effects of losses of the material under test (MUT) on sensitivity have been considered in the analysis. It has been found that, depending on the level of losses of the MUT and the number of high/low inverter stages, sensor operation proceeds either under the so-called low-loss regime, or under the high-loss regime. In one case, the sensitivity, defined as the derivative of the phase of the reflection coefficient at the operating frequency with the dielectric constant of the MUT, is negative (low-loss mode), whereas it is positive under operation in the high-loss regime. In both cases, the sensitivity in the vicinity of small perturbations can be optimized through a proper design, mainly controlled by the admittances of the inverter stages, as corroborated by the two designed and fabricated prototypes. One of such prototypes has been focused on the dielectric

characterization of low-loss solid samples. The maximum sensitivity in such prototype has been found to be 255.5º, a competitive value, taking into account that the device has been implemented with a single inverter stage. The second prototype is a sensor devoted to the measurement of the concentration of isopropanol in diluted solutions of isopropanol in deionized (DI) water. Contrary to the previous prototype, this second prototype sensor, dealing with lossy dielectrics (i.e., mixtures of isopropanol and DI water), operates under the high-loss regime. This liquid sensor exhibits a maximum sensitivity of 64.96º/%, a competitive value despite the high level of losses of the considered MUTs. Moreover, the sensor is able to discern volume fractions of isopropanol (resolution) as small as 0.5 %. This is a very good resolution, intimately related to the high-achieved sensitivity. The fact that the sensing element is a slot resonator (etched in the ground plane), also a novel aspect of the proposed sensor, facilitates the addition of the mechanical accessories (e.g., the holder), and precludes any interaction of the MUT with the microwave circuitry (i.e., the inverter stages). The reason is that such elements (holder and MUT) are backside isolated from the upper metallic layer of the microstrip structure. It can be envisaged that the sensors proposed in the present paper can find practical application in a variety of scenarios requiring the accurate measurement of the dielectric properties of materials, or other physical or chemical variables related to the permittivity (presence of impurities in samples, material composition, physical variables, such as temperature, or humidity, etc.).

REFERENCES

[1] F. Martín, P. Vélez, J. Muñoz-Enano, L. Su, *Planar Microwave Sensors*, Wiley/IEEE Press, Hoboken, NJ, USA, 2022.

[2] M. Abdolrazzaghi, V. Nayyeri, F. Martín, "Techniques to Improve the Performance of Planar Microwave Sensors: A Review and Recent Developments", *Sensors*, vol. 22, paper 6946, 2022.

[3] J. Muñoz-Enano, P. Vélez, L. Su, M. Gil, P. Casacuberta, and F. Martín, "On the sensitivity of reflective-mode phase variation sensors based on open-ended stepped-impedance transmission lines: theoretical analysis and experimental validation", *IEEE Trans. Microw. Theory Techn*. vol. 69, no. 1, pp. 308-324, Jan. 2021.

[4] C. Damm, M. Schussler, M. Puentes, H. Maune, M. Maasch and R. Jakoby, "Artificial transmission lines for high sensitive microwave sensors," *IEEE Sensors Conf.,* Christchurch, New Zealand, pp. 755−758, Oct. 2009.

[5] F.J. Ferrández-Pastor, J.M. García-Chamizo and M. Nieto-Hidalgo, "Electromagnetic differential measuring method: application in microstrip sensors developing", Sensors, vol. 17, p. 1650, 2017.

[6] J. Muñoz-Enano, P. Vélez, M. Gil, F. Martín, "An analytical method to implement high sensitivity transmission line differential sensors for dielectric constant measurements", *IEEE Sensors J.*, vol. 20, pp. 178-184, Jan. 2020.

[7] M. Gil, P. Vélez, F. Aznar, J. Muñoz-Enano, and F. Martín, "Differential sensor based on electro-inductive wave (EIW) transmission lines for dielectric constant measurements and defect detection", *IEEE Trans. Ant. Propag*., vol. 68, pp. 1876-1886, Mar. 2020.

[8] J. Muñoz-Enano, P. Vélez, M. Gil, J. Mata-Contreras, and F. Martín, "Differential-mode to common-mode conversion detector based on rat-race couplers: analysis and application to microwave sensors and comparators", *IEEE Trans. Microw. Theory Techn*., vol. 68, pp. 1312-1325, Apr. 2020.

[9] J. Coromina, J. Muñoz-Enano, P. Vélez, A. Ebrahimi, J. Scott, K. Ghorbani, F. Martín, "Capacitively-Loaded Slow-Wave Transmission Lines for Sensitivity Improvement in Phase-Variation Permittivity Sensors", *50th Europ. Microw. Conf*., Utrecht, The Netherlands Sep. 2020.

[10] A. Ebrahimi, J. Coromina, J. Muñoz-Enano, P. Vélez, J. Scott, K. Ghorbani, and F. Martín, "Highly Sensitive Phase-Variation Dielectric Constant Sensor Based on a Capacitively-Loaded Slow-Wave Transmission Line," *IEEE Trans. Circ. Syst. I: Reg. Papers*, vol. 68, no. 7, pp. 2787-2799, Jul. 2021.

[11] L. Su, J. Muñoz-Enano, P. Vélez, P. Casacuberta, M. Gil, F. Martín, "Phase-Variation Microwave Sensor for Permittivity Measurements Based on a High-Impedance Half-Wavelength Transmission Line," *IEEE Sensors J*., vol. 21, no. 9, pp. 10647-10656, May 2021.

[12] A. K. Jha, A. Lamecki, M. Mrozowski, and M. Bozzi, "A highly sensitive planar microwave sensor for detecting direction and angle of rotation," *IEEE Trans. Microw. Theory Techn*., vol. 68, no. 4, pp. 1598–1609, Apr. 2020.

[13] L. Su, J. Muñoz-Enano, P. Velez, P. Casacuberta, M. Gil and F. Martin, "Highly Sensitive Phase Variation Sensors Based on Step-Impedance Coplanar Waveguide (CPW) Transmission Lines," *IEEE Sensors J*., vol. 21, no. 3, pp. 2864-2872, Feb. 2021.

[14] P. Casacuberta, J. Muñoz-Enano, P. Vélez, L. Su, M. Gil, and F. Martín, "Highly sensitive reflective-mode detectors and dielectric constant sensors based on open-ended stepped-impedance transmission lines", *Sensors*, vol. 20, paper 6236, 2020.

[15] L. Su, J. Muñoz-Enano, P. Vélez, M. Gil, P. Casacuberta, and F. Martín, "Highly sensitive reflective-mode phase-variation permittivity sensor based on a coplanar waveguide (CPW) terminated with an open complementary split ring resonator (OCSRR)," *IEEE Access*, vol. 9, pp. 27928-27944, 2021.

[16] P. Casacuberta, P. Vélez, J. Muñoz-Enano, L. Su, M. Gil, A. Ebrahimi and F. Martín, "Circuit analysis of a Coplanar waveguide (CPW) terminated with a step-impedance resonator (SIR) for highly sensitive one-port permittivity sensing," *IEEE Access*, vol. 10, pp. 62597-62612, 2022.

[17] A. K. Horestani, Z. Shaterian and F. Martín, "Rotation Sensor Based on the Cross-Polarized Excitation of Split Ring Resonators (SRRs)", *IEEE Sensors J*., vol 20, pp. 9706-9714, Sep. 2020.

[18] J. Muñoz-Enano, P. Vélez, L. Su, M. Gil, and F. Martín, "A reflective-mode phase-variation displacement sensor", *IEEE Access*, vol. 8, pp. 189565-189575, Oct. 2020.

[19] P. Casacuberta, P. Vélez, J. Muñoz-Enano, L. Su, and F. Martín "Highly sensitive reflective-mode phase-variation permittivity sensors using coupled line sections", *IEEE Trans. Microw. Theory Techn*., vol. 71, no. 7, pp. 2970-2984, Jul. 2023.

[20] P. Casacuberta, P. Vélez, J. Muñoz-Enano, L. Su, M. Gil-Barba, and F. Martín, "Reflective-Mode Phase-Variation Permittivity Sensors Based on Coupled Resonators", *IEEE Sensors 2022*, Dallas, Texas, USA, Oct. 30 - Nov. 2, 2022.

[21] M. Puentes, C. Weiß, M. Schüßler, and R. Jakoby, "Sensor array based on split ring resonators for analysis of organic tissues," in *IEEE MTT-S Int. Microw. Symp.*, Baltimore, MD, USA, Jun. 2011, pp. 1−4.

[22] B. Ebrahimi, W. Withayachumnankul, S. Al-Sarawi, D. Abbott, "High-sensitivity metamaterial-inspired sensor for microfluidic dielectric characterization," *IEEE Sensors J.*, vol. 14, no. 5, pp. 1345−1351, May 2014.

[23] M. Schüßler, C. Mandel, M. Puentes, and R. Jakoby, "Metamaterial inspired microwave sensors," *IEEE Microw. Mag.*, vol. 13, no. 2, pp. 57–68, Mar. 2012.

[24] M. S. Boybay and O. M. Ramahi, "Material characterization using complementary split-ring resonators," *IEEE Trans. Instrum. Meas*., vol. 61, no. 11, pp. 3039−3046, Nov. 2012.

[25] C.-S. Lee and C.-L. Yang, "Complementary split-ring resonators for measuring dielectric constants and loss tangents," *IEEE Microw. Wireless Compon. Lett.*, vol. 24, no. 8, pp. 563−565, Aug. 2014.

[26] C.-L. Yang, C.-S. Lee, K.-W. Chen, and K.-Z. Chen, "Noncontact measurement of complex permittivity and thickness by using planar resonators," *IEEE Trans. Microw. Theory Techn.*, vol. 64, no.1, pp. 247−257, Jan. 2016.

[27] L. Su, J. Mata-Contreras, P. Vélez, F. Martín, "Estimation of the complex permittivity of liquids by means of complementary split ring resonator (CSRR) loaded transmission lines", *2017 IEEE MTT-S International Microwave Workshop Series on Advanced Materials and Processes* (IMWS-AMP 2017), Pavia, Italy, 20-22 Sep. 2017.

[28] L. Su, J. Mata-Contreras, P. Vélez, B. Fernández-Prieto and F. Martín, "Analytical method to estimate the complex permittivity of oil Samples", *Sensors*, 18(4), paper 984, 2018.

[29] B.K, Jha, N, Delmonte, A, Lamecki, M, Mrozowski, M, Bozzi, "Design of microwave-based angular displacement sensor", *IEEE Microw. Wireless Compon. Lett.*, vol. 29 (4), pp. 306-308, Apr. 2019.
[30] M. Saadat-Safa, V. Nayyeri, M. Khanjarian, M. Soleimani and O. M. Ramahi, "A CSRR-Based Sensor for Full Characterization of Magneto-Dielectric Materials," *IEEE Trans. Microw. Theory Techn*., vol. 67, no. 2, pp. 806-814, Feb. 2019.
[31] J. Muñoz-Enano, P. Vélez, M. Gil, F. Martín, "Frequency variation sensors for permittivity measurements based on dumbbell-shaped defect ground structures (DB-DGS): analytical method and sensitivity analysis", *IEEE Sensors J*., vol. 22, no. 10, pp. 9378-9386, May 2022.
[32] J. Naqui, C. Damm, A. Wiens, R. Jakoby, L. Su, J. Mata-Contreras, and F. Martín, "Transmission Lines Loaded with Pairs of Stepped Impedance Resonators: Modeling and Application to Differential Permittivity Measurements", *IEEE Trans. Microw. Theory Techn*., vol. 64, no. 11, pp. 3864-3877, Nov. 2016.
[33] L. Su, J. Mata-Contreras, J. Naqui, and F. Martín, "Splitter/combiner microstrip sections loaded with pairs of complementary split ring resonators (CSRRs): modeling and optimization for differential sensing applications", *IEEE Trans. Microw. Theory Techn*, vol. 64(12), pp. 4362-4370, Dec. 2016
[34] P. Vélez, L. Su, K. Grenier, J. Mata-Contreras, D. Dubuc, and F. Martín, "Microwave microfluidic sensor based on a microstrip splitter/combiner configuration and split ring resonators (SRR) for dielectric characterization of liquids", *IEEE Sensors J*., vol. 17, pp. 6589-6598, Oct. 2017.
[35] A. Ebrahimi, J. Scott, and K. Ghorbani, "Differential sensors using microstrip lines loaded with two split-ring resonators," *IEEE Sens. J*., vol. 18, pp. 5786-5793, 2018.
[36] A. Ebrahimi, G. Beziuk, J. Scott, and K. Ghorbani, "Microwave differential frequency splitting sensor using magnetic-LC resonators," *Sensors*, vol. 20, p. 1066, 2020.
[37] J. Naqui, M. Durán-Sindreu and F. Martín, "Novel sensors based on the symmetry properties of split ring resonators (SRRs)," *Sensors*, vol 11, pp. 7545−7553, 2011.
[38] J. Naqui, M. Durán-Sindreu, and F. Martín, "Alignment and position sensors based on split ring resonators," *Sensors*, vol. 12, pp. 11790−11797, 2012.
[39] B.K. Horestani, C. Fumeaux, S.F. Al-Sarawi, and D. Abbott, "Displacement sensor based on diamond-shaped tapered split ring resonator," *IEEE Sens. J*., vol. 13, pp. 1153–1160, 2013.
[40] B.K. Horestani, D. Abbott, and C. Fumeaux, "Rotation sensor based on horn-shaped split ring resonator," *IEEE Sens. J.*, vol. 13, pp. 3014–3015, 2013.
[41] J. Naqui and F. Martín, "Transmission lines loaded with bisymmetric resonators and their application to angular displacement and velocity sensors," *IEEE Trans. Microw. Theory Techn*., vol. 61, no. 12, pp. 4700–4713, Dec. 2013.
[42] J. Naqui and F. Martín, "Angular displacement and velocity sensors based on electric-LC (ELC) loaded microstrip lines," *IEEE Sensors J.*, vol. 14, no. 4, pp. 939–940, Apr. 2014.
[43] B.K. Horestani, J. Naqui, D. Abbott, C. Fumeaux, and F. Martín, "Two-dimensional displacement and alignment sensor based on reflection coefficients of open microstrip lines loaded with split ring resonators," *Elec. Lett*., vol. 50, pp. 620–622, Apr. 2014.
[44] B. Ebrahimi, W. Withayachumnankul, S. F. Al-Sarawi and D. Abbott, "Metamaterial-Inspired Rotation Sensor With Wide Dynamic Range," *IEEE Sensors J*., vol. 14, no. 8, pp. 2609-2614, Aug. 2014.
[45] J. Naqui, J. Coromina, B. Karami-Horestani, C. Fumeaux, and F. Martín, "Angular displacement and velocity sensors based on coplanar waveguides (CPWs) loaded with S-shaped split ring resonator (S-SRR)," *Sensors*, vol. 15, pp. 9628–9650, 2015.
[46] J. Mata-Contreras, C. Herrojo, and F. Martín, "Application of split ring resonator (SRR) loaded transmission lines to the design of angular displacement and velocity sensors for space applications", *IEEE Trans. Microw. Theory Techn*., vol. 65, no. 11, pp. 4450-4460, Nov. 2017.
[47] J. Mata-Contreras, C. Herrojo, and F. Martín, "Detecting the rotation direction in contactless angular velocity sensors implemented with rotors loaded with multiple chains of split ring resonators (SRRs)", *IEEE Sensors J*., vol.18, no. 17, pp. 7055-7065, Sep. 2018.
[48] P. Vélez, J. Muñoz-Enano, A. Ebrahimi, C. Herrojo, F. Paredes, J. Scott, K. Ghorbani, and F. Martín, "Single-Frequency Amplitude-Modulation Sensor for Dielectric Characterization of Solids and Microfluidics", *IEEE Sensors J*., vol. 21, no. 10, pp. 12189-12201, May 2021.
[49] A. M. Albishi, M. K. E. Badawe, V. Nayyeri, and O. M. Ramahi, "Enhancing the Sensitivity of Dielectric Sensors With Multiple Coupled Complementary Split-Ring Resonators," *IEEE Trans. Microw. Theory Tech.*, vol. 68, no. 10, pp. 4340–4347, Oct. 2020.
[50] M. Abdolrazzaghi, M. Daneshmand, and A. K. Iyer, "Strongly Enhanced Sensitivity in Planar Microwave Sensors Based on Metamaterial Coupling," *IEEE Trans. Microw. Theory Tech*., vol. 66, no. 4, pp. 1843–1855, Apr. 2018.
[51] C. G. Juan, B. Potelon, C. Quendo, E. Bronchalo, and J. M. Sabater-Navarro, "Highly-Sensitive Glucose Concentration Sensor Exploiting Inter-resonators Couplings," *2019 49th European Microwave Conference* (EuMC), Oct. 2019, pp. 662–665.
[52] Z. Xu, Y. Wang, and S. Fang, "Dielectric Characterization of Liquid Mixtures Using EIT-like Transmission Window," *IEEE Sensors J*., vol. 21, no. 16, pp. 17 859–17 867, Aug. 2021.
[53] I. Piekarz, J. Sorocki, K. Wincza, and S. Gruszczynski, "Microwave Sensors for Dielectric Sample Measurement Based on Coupled-Line Section," *IEEE Trans. Microw. Theory Tech*., vol. 65, no. 5, pp. 1615–1631, May 2017.
[54] J. Sorocki, I. Piekarz, K. Wincza, S. Gruszczynski, and J. Papapolymerou, "Broadband Microwave Microfluidic Coupled-Line Sensor With 3-D-Printed Channel for Industrial Applications," *IEEE Trans. Microw. Theory Tech*., vol. 68, no. 7, pp. 2808–2822, Jul. 2020.
[55] I. Piekarz, J. Sorocki, K. Wincza, and S. Gruszczynski, "Coupled-Line Sensor with Marchand Balun as RF System for Dielectric Sample Detection," *IEEE Sensors J*., vol. 16, no. 1, pp. 88–96, Jan. 2016.
[56] Z. R. Omam, V. Nayyeri, and O. M. Ramahi, "Microstrip Coupled-Line Directional Coupler for High-Sensitivity Dielectric Constant Measurement," *2021 51st Europ. Microw. Conf.* (EuMC), Apr. 2022, pp. 413–416.
[57] Z. R. Omam, V. Nayyeri, S. -H. Javid-Hosseini and O. M. Ramahi, "Simple and High-Sensitivity Dielectric Constant Measurement Using a High-Directivity Microstrip Coupled-Line Directional Coupler," *IEEE Trans. Microw. Theory Techn*., vol. 70, no. 8, pp. 3933-3942, Aug. 2022.
[58] J. Muñoz-Enano, P. Vélez, P. Casacuberta, L. Su, and F. Martín, "Characterization of the quality of edible oils subjected to industrial frying processes through high sensitivity microwave sensors", *53rd Europ. Microw. Conf.*, Berlin, Germany, 17-22 Sep. 2023.
[59] J. Muñoz-Enano, J. Martel, P. Vélez, F. Medina, L. Su, and F. Martín, "Parametric analysis of the edge capacitance of uniform slots and application to frequency-variation permittivity sensors", *Appl. Sci.*, vol. 11, paper 7000, 2021.

Jonathan Muñoz-Enano (S'19) was born in Mollet del Vallès (Barcelona), Spain, in 1994. He received the Bachelor's Degree in Electronic Telecommunications Engineering in 2016 and the Master's Degree in Telecommunications Engineering in 2018, both at the Autonomous University of Barcelona (UAB). In July 2022, he obtained the PhD degree within the doctoral programme in Electronics Engineering and Telecommunications in the same university, with the thesis entitled "Highly Sensitive Planar Microwave Sensors for Dielectric Characterization of Solids, Liquids, and Biosamples." Actually, he is working as a postdoctoral researcher at CIMITEC, Universitat Autònoma de Barcelona.

Paris Vélez (S'10–M'14) was born in Barcelona, Spain, in 1982. He received the degree in Telecommunications Engineering, specializing in electronics, the Electronics Engineering degree, and the Ph.D. degree in Electrical Engineering from the Universitat Autònoma de Barcelona, Barcelona, in 2008, 2010, and 2014, respectively. His Ph.D. thesis concerned common mode suppression differential microwave circuits based on metamaterial concepts and semi-lumped resonators. During the Ph.D., he was awarded with a pre-doctoral teaching and research fellowship by the Spanish Government from 2011 to 2014. From 2015-2017, he was involved in the subjects related to metamaterials sensors for fluidics detection and characterization at LAAS-CNRS through a TECNIOSpring fellowship cofounded by the Marie Curie program. His current research interests include the miniaturization of passive circuits RF/microwave and sensors-based metamaterials through Juan de la Cierva fellowship. Dr. Vélez is a Reviewer for the IEEE Transactions on Microwave Theory and Techniques and for other journals.

Pau Casacuberta (GS'22) was born in Sabadell (Barcelona), Spain, in 1997. He received the Bachelor's Degree in Electronic Telecommunications Engineering and Computer Engineering from the Universitat Autònoma de Barcelona (UAB) in 2020, and the master's degree in Telecommunications Engineering in 2022. He received the Collaboration fellowship by the Spanish Government in 2019 for developing his Bachelor's Thesis in highly sensitive microwave sensors based in stepped impedance structures. Furthermore, he is currently working in the elaboration of his PhD, which is focused on the development of microwave sensors for the characterization of the composition of multicomponent liquid substances, with a research grant from FPU Program of the Universities Spanish Ministry.

Lijuan Su was born in Qianjiang (Hubei), China in 1983. She received the B.S. degree in communication engineering and the M.S. degree in circuits and systems both from Wuhan University of Technology, Wuhan, China, in 2005 and 2013 respectively, and the Ph.D. degree in electronic engineering from Universitat Autonoma de Barcelona, Barcelona, Spain, in 2017. From Nov. 2017 to Dec. 2019, she worked as a postdoc researcher in Flexible Electronics Research Center, Huazhong University of Science and Technology, Wuhan, China. She is currently a postdoc researcher in CIMITEC, Universitat Autonoma de Barcelona, Spain. Her current research interests focus on the development of novel microwave sensors with improved performance for biosensors, dielectric characterization of solids and liquids, defect detection, industrial processes, etc.

Ferran Martín (M'04-SM'08-F'12) was born in Barakaldo (Vizcaya), Spain in 1965. He received the B.S. Degree in Physics from the Universitat Autònoma de Barcelona (UAB) in 1988 and the PhD degree in 1992. From 1994 up to 2006 he was Associate Professor in Electronics at the Departament d'Enginyeria Electrònica (Universitat Autònoma de Barcelona), and since 2007 he is Full Professor of Electronics. In recent years, he has been involved in different research activities including modelling and simulation of electron devices for high frequency applications, millimeter wave and THz generation systems, and the application of electromagnetic bandgaps to microwave and millimeter wave circuits. He is now very active in the field of metamaterials and their application to the miniaturization and optimization of microwave circuits and antennas. Other topics of interest include microwave sensors and RFID systems, with special emphasis on the development of high data capacity chipless-RFID tags. He is the head of the Microwave Engineering, Metamaterials and Antennas Group (GEMMA Group) at UAB, and director of CIMITEC, a research Center on Metamaterials supported by TECNIO (Generalitat de Catalunya). He has organized several international events related to metamaterials and related topics, including Workshops at the IEEE International Microwave Symposium (years 2005 and 2007) and European Microwave Conference (2009, 2015 and 2017), and the Fifth International Congress on Advanced Electromagnetic Materials in Microwaves and Optics (Metamaterials 2011), where he acted as Chair of the Local Organizing Committee. He has acted as Guest Editor for six Special Issues on metamaterials and sensors in five International Journals. He has authored and co-authored over 650 technical conference, letter, journal papers and book chapters, he is co-author of the book on Metamaterials entitled *Metamaterials with Negative Parameters: Theory, Design and Microwave Applications* (John Wiley & Sons Inc.), author of the book *Artificial Transmission Lines for RF and Microwave Applications* (John Wiley & Sons Inc.), co-editor of the book *Balanced Microwave Filters* (Wiley/IEEE Press), co-author of the book *Time-Domain Signature Barcodes for Chipless-RFID and Sensing Applications* (Springer), and co-author of the book *Planar Microwave Sensors* (Wiley/IEEE Press). Ferran Martín has generated 22 PhDs, has filed several patents on metamaterials and has headed several Development Contracts.

Prof. Martín is a member of the IEEE Microwave Theory and Techniques Society (IEEE MTT-S). He is reviewer of the IEEE Transactions on Microwave Theory and Techniques and IEEE Microwave and Wireless Components Letters, among many other journals, and he serves as member of the Editorial Board of IET Microwaves, Antennas and Propagation, International Journal of RF and Microwave Computer-Aided Engineering, and Sensors. He is also a member of the Technical Committees of the European Microwave Conference (EuMC) and International Congress on Advanced Electromagnetic Materials in Microwaves and Optics (Metamaterials). Among his distinctions, Ferran Martín has received the 2006 Duran Farell Prize for Technological Research, he holds the *Parc de Recerca UAB – Santander* Technology Transfer Chair, and he has been the recipient of three ICREA ACADEMIA Awards (calls 2008, 2013 and 2018). He is Fellow of the IEEE and Fellow of the IET.